54

Cardiac Biomechanics

Andrew D. McCulloch
University of California

54.1 Introduction

The primary function of the heart, to pump blood through the circulatory system, is fundamentally mechanical. In this chapter, cardiac function is discussed in the context of the mechanics of the ventricular walls from the perspective of the determinants of myocardial stresses and strains (Table 54.1). Many physiological, pathophysiological, and clinical factors are directly or indirectly affected by myocardial stress and strain (Table 54.2). Of course, the factors in Tables 54.1 and 54.2 are closely interrelated — most of the factors affected by myocardial stress and strain in turn affect the stress and strain in the ventricular wall. For example, changes in wall stress due to altered hemodynamic load may cause ventricular remodeling, which in turn alters geometry, structure, and material properties. This chapter is organized around the governing determinants in Table 54.1, but mention is made where appropriate to some of the factors in Table 54.2.

54.2 Cardiac Geometry and Structure

The mammalian heart consists of four pumping chambers, the left and right atria and ventricles communicating through the atrioventricular (mitral and tricuspid) valves, which are structurally connected by chordae tendineae to papillary muscles that extend from the anterior and posterior aspects of the right and left ventricular lumens. The muscular cardiac wall is perfused via the coronary vessels that originate at the left and right coronary ostia located in the sinuses of Valsalva immediately distal to the aortic valve leaflets. Surrounding the whole heart is the collagenous parietal pericardium that fuses with

JOBR: "2121_c054" — 2005/11/11 — 17:45 — page 1 — #1

TABLE 54.1 Basic Determinants of Myocardial Stress and Strain

Geometry and structure	
Three-dimensional shape	Wall thickness
	Curvature
	Stress-free and unloaded reference configurations
Tissue structure	Muscle fiber architecture
	Connective tissue organization
	Pericardium, epicardium, and endocardium
	Coronary vascular anatomy
Boundary/initial conditions	
Pressure	Filling pressure (preload)
	Arterial pressure (afterload)
	Direct and indirect ventricular interactions
	Thoracic and pericardial pressure
Constraints	Effects of inspiration and expiration
	Constraints due to the pericardium and its attachments
	Valves and fibrous valve annuli, chordae tendineae
	Great vessels, lungs
Material properties	
Resting or passive	Nonlinear finite elasticity
	quasilinear viscoelasticity
	Anisotropy
	Biphasic poroelasticity
Active dynamic	Activation sequence
	Myofiber isometric and isotonic contractile dynamics
	Sarcomere length and length history
	Cellular calcium kinetics and metabolic energy supply

TABLE 54.2 Factors Affected by Myocardial Stress and Strain

Direct factors	Regional muscle work
	Myocardial oxygen demand and energetics
	Coronary blood flow
Electrophysiological responses	Action potential duration (QT interval)
	Repolarization (T wave morphology)
	Excitability
	Risk of arrhythmia
Development and morphogenesis	Growth rate
	Cardiac looping and septation
	Valve formation
Vulnerability to injury	Ischemia
	Arrhythmia
	Cell dropout
	Aneurysm rupture
Remodeling, repair and adaptation	Eccentric and concentric hypertrophy
	Fibrosis
	Scar formation
Progression of disease	Transition from hypertrophy to failure
	Ventricular dilation
	Infarct expansion
	Response to reperfusion
	Aneurysm formation

TABLE 54.3 Representative Left Ventricular Minor-Axis Dimensions[a]

Species	Comments	Inner radius (mm)	Outer radius (mm)	Wall thickness: inner radius
Dog (21 kg)	Unloaded diastole (0 mmHg)	16	26	0.62
	Normal diastole (2–12 mmHg)	19	28	0.47
	Dilated diastole (24–40 mmHg)	22	30	0.36
	Normal systole (1–9 mmHg EDP)	14	26	0.86
	Long axis, apex-equator (normal diastole)	42	47	0.12
Young rats	Unloaded diastole (0 mmHg)	1.4	3.5	1.50
Mature rats	Unloaded diastole (0 mmHg)	3.2	5.8	0.81
Human	Normal	24	32	0.34
	Compensated pressure overload	27	42	0.56
	Compensated volume overload	32	42	0.33

[a] Dog data from Ross et al. [129], and Streeter and Hanna [2]. Human data from Grossman et al. [130,131]. Rat data are from unpublished observations in the author's laboratory.

the diaphragm and great vessels. These are the anatomical structures that are most commonly studied in the field of cardiac mechanics. Particular emphasis in this chapter is given to the ventricular walls, which are the most important for the pumping function of the heart. Most studies of cardiac mechanics have focused on the left ventricle, but many of the important conclusions apply equally to the right ventricle.

54.2.1 Ventricular Geometry

From the perspective of engineering mechanics, the ventricles are three-dimensional thick-walled pressure vessels with substantial variations in wall thickness and principal curvatures both regionally and temporally through the cardiac cycle. The ventricular walls in the normal heart are thickest at the equator and base of the left ventricle and thinnest at the left ventricular apex and right ventricular free wall. There are also variations in the principal dimensions of the left ventricle with species, age, phase of the cardiac cycle, and disease (Table 54.3). But, in general, the ratio of wall thickness to radius is too high to be treated accurately by all but the most sophisticated thick-wall shell theories [1].

Ventricular geometry has been studied in most quantitative detail in the dog heart [2,3]. Geometric models have been very useful in the analysis, especially the use of confocal and nonconfocal ellipses of revolution to describe the epicardial and endocardial surfaces of the left and right ventricular walls (Figure 54.1). The canine left ventricle is reasonably modeled by a thick ellipsoid of revolution truncated at the base. The crescentic right ventricle wraps about 180° degrees around the heart wall circumferentially and extends longitudinally about two-thirds of the distance from the base to the apex. Using a truncated ellipsoidal model, left ventricular geometry in the dog can be defined by the major and minor radii of two surfaces, the left ventricular endocardium, and a surface defining the free wall epicardium and the septal endocardium of the right ventricle. Streeter and Hanna [2] described the position of the basal plane using a truncation factor f_b defined as the ratio between the longitudinal distances from equator-to-base and equator-to-apex. Hence, the overall longitudinal distance from base to apex is $(1 + f_b)$ times the major radius of the ellipse. Since variations in f_b between diastole and systole are relatively small (0.45 to 0.51), they suggested a constant value of 0.5.

The focal length d of an ellispoid is defined from the major and minor radii (a and b) by $d^2 = a^2 – b^2$, and varies only slightly in the dog from endocardium to epicardium between end-diastole (37.3 to 37.9 mm) and end-systole (37.7 to 37.1 mm) [2]. Hence, within the accuracy that the boundaries of the left ventricular wall can be treated as ellipsoids of revolution, the assumption that the ellipsoids are confocal appears to be a good one. This has motivated the choice of prolate spheroidal (elliptic-hyperbolic-polar) coordinates (λ, μ, θ) as a system for economically representing ventricular geometries obtained postmortem or by noninvasive tomography [3,4]. The Cartesian coordinates of a point are given in terms of its prolate

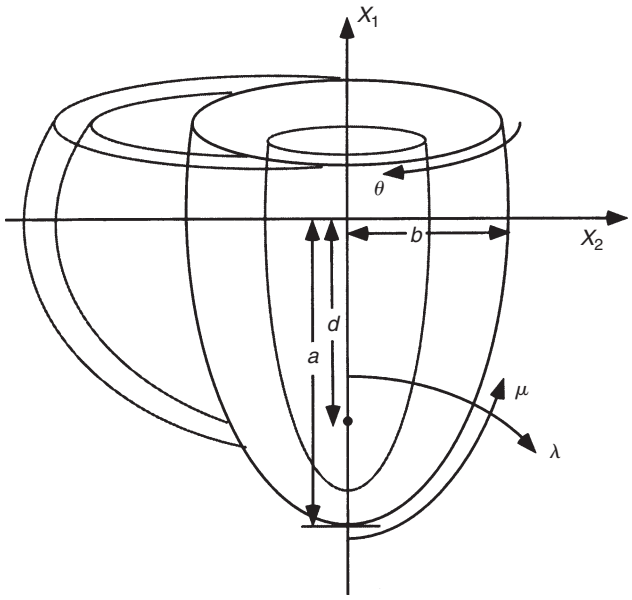

FIGURE 54.1 Truncated ellipsoid representation of ventricular geometry, showing major left ventricular radius (a), minor radius (b), focal length (d) and prolate spheroidal coordinates (λ, μ, θ).

spheroidal coordinates by

$$\begin{aligned} x_1 &= d \cosh\lambda \cos\mu, \\ x_2 &= d \sinh\lambda \sin\mu \cos\theta, \\ x_3 &= d \sinh\lambda \sin\mu \sin\theta \end{aligned} \tag{54.1}$$

Here, the focal length d defines a family of coordinate systems that vary from spherical polar when $d = 0$ to cylindrical polar in the limit when $d \to \infty$. A surface of constant transmural coordinate λ (Figure 54.1) is an ellipse of revolution with major radius $a = d \cosh\lambda$ and minor radius $b = d \sinh\lambda$. In an ellipsoidal model with a truncation factor of 0.5, the longitudinal coordinate μ varies from zero at the apex to 120° at the base. Integrating the Jacobian in prolate spheroidal coordinates gives the volume of the wall or cavity:

$$\begin{aligned} & d^3 \int_0^{2\pi} \int_0^{\mu_2} \int_{\lambda_1}^{\lambda_2} ((\sinh^2\lambda + \sin^2\mu) \sinh\lambda \sin\mu) \mathrm{d}\lambda \, \mathrm{d}\mu \, \mathrm{d}\theta \\ &= \frac{2\pi d^3}{3} \left| (1 - \cos\mu_2) \cosh^3\lambda - (1 - \cos^3\mu_2) \cosh\lambda \right|_{\lambda_1}^{\lambda^2} \end{aligned} \tag{54.2}$$

The scaling between heart mass M_H and body mass M within or between species is commonly described by the allometric formula,

$$M_H = kM^{\alpha} \tag{54.3}$$

Using combined measurements from a variety of mammalian species with M expressed in kilograms, the coefficient k is 5.8 g and the power α is close to unity (0.98) [5]. Within individual species, the ratio of heart weight to body weight is somewhat lower in mature rabbits and rats (about 2 g/kg) than in humans (5 g/kg) and higher in horses and dogs (8 g/kg) [6]. The rate α of heart growth with body weight decreases with age in most species but not in humans. At birth, left and right ventricular weights are similar, but the left ventricle is substantially more massive than the right by adulthood.

54.2.2 Myofiber Architecture

The cardiac ventricles have a complex three-dimensional muscle fiber architecture (for a comprehensive review see Streeter) [7]. Although the myocytes are relatively short, they are connected such that at any point in the normal heart wall there is a clear predominant fiber axis that is approximately tangent with the wall (within 3 to 5° in most regions, except near the apex and papillary muscle insertions). Each ventricular myocyte is connected via gap junctions at intercalated disks to an average of 11.3 neighbors, 5.3 on the sides and 6.0 at the ends [8]. The classical anatomists dissected discrete bundles of fibrous swirls, though later investigations showed that the ventricular myocardium could be unwrapped by blunt dissection into a single continuous muscle "ban" [9]. However, more modern histological techniques have shown that in the plane of the wall, the mean muscle fiber angle makes a smooth transmural transition from epicardium to endocardium (Figure 54.2). About the mean, myofiber angle dispersion is typically 10 to 15° [10] except in certain pathologies. Similar patterns have been described for humans, dogs, baboons, macaques, pigs, guinea pigs, and rats. In the left ventricle of humans or dogs, the muscle fiber angle typically varies continuously from about −60° (i.e., 60° clockwise from the circumferential axis) at the epicardium to about +70° at the endocardium. The rate of change of fiber angle is usually greatest at the epicardium, so that circumferential (0°) fibers are found in the outer half of the wall, and begins to slow approaching the inner third near the trabeculata–compacta interface. There are also small increases in fiber orientation from end-diastole to systole (7 to 19°), with greatest changes at the epicardium and apex [11].

Regional variations in ventricular myofiber orientations are generally smooth except at the junction between the right ventricular free wall and septum. A detailed study in the dog that mapped fiber angles throughout the entire right and left ventricles described the same general transmural pattern in all regions including the septum and right ventricular free wall, but with definite regional variations [3]. Transmural differences in fiber angle were about 120 to 140° in the left ventricular free wall, larger in the septum (160 to 180°) and smaller in the right ventricular free wall (100 to 120°). A similar study of fiber angle distributions in the rabbit left and right ventricles has recently been reported [12]. For the most part, fiber angles in the rabbit heart were very similar to those in the dog, except for on the anterior wall, where average fiber orientations were 20 to 30° counterclockwise of those in the dog. While the most reliable reconstructions of ventricular myofiber architecture have been made using quantitative histological techniques, diffusion tensor magnetic resonance imaging (MRI) has proven to be a reliable technique for estimating fiber orientation nondestructively in fixed [13,14] and even intact beating human hearts [15].

The locus of fiber orientations at a given depth in the ventricular wall has a spiral geometry that may be modeled as a general helix by simple differential geometry. The position vector $\mathbf{x}$ of a point on a helix inscribed on an ellipsoidal surface that is symmetric about the x_1 axis and has major and minor radii, a and b, is given by the parametric equation,

$$\mathbf{x} = a \sin t \boldsymbol{e}_1 + b \cos t \sin wt \boldsymbol{e}_2 + b \cos t \cos wt \boldsymbol{e}_3 \tag{54.4}$$

where the parameter is t, and the helix makes $w/4$ full turns between apex and equator. A positive w defines a left-handed helix with a positive pitch. The fiber angle or helix pitch angle η, varies along the arc length:

$$\sin \eta = \sqrt{\frac{a^2 \cos^2 t + b^2 \sin^2 t}{(a^2 + b^2 w^2) \cos^2 t + b^2 \sin^2 t}} \tag{54.5}$$

If another, deformed configuration $\hat{\mathbf{x}}$ is defined in the same way as Equation (54.4), the fiber-segment-extension ratio $\mathrm{d}\hat{s}/\mathrm{d}s$ associated with a change in the ellipsoid geometry [16] can be derived from

$$\frac{\mathrm{d}\hat{s}/\mathrm{d}t}{\mathrm{d}s/\mathrm{d}t} = \frac{|\mathrm{d}\hat{x}/\mathrm{d}t|}{|\mathrm{d}x/\mathrm{d}t|} \tag{54.6}$$

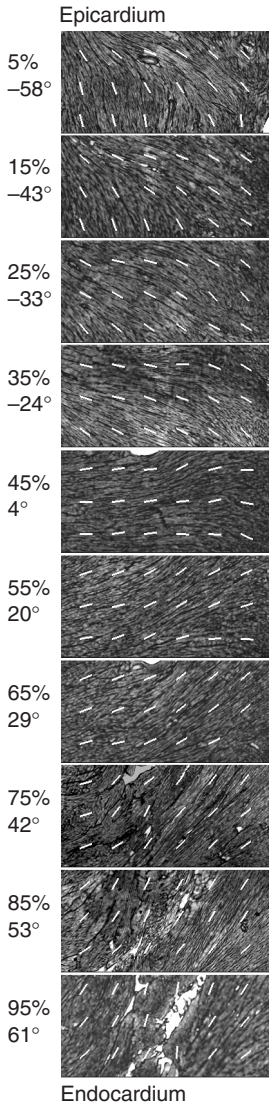

FIGURE 54.2 Cardiac muscle fiber orientations vary continuously through the left ventricular wall from a negative angle at the epicardium (0%) to near zero (circumferential) at the midwall (50%) and to increasing positive values toward the endocardium (100%). (Courtesy Jyoti Rao, Micrographs of murine myocardium from the author's laboratory.)

Although the traditional notion of discrete myofiber bundles has been revised in view of the continuous transmural variation of muscle fiber angle in the plane of the wall, there is a transverse laminar structure in the myocardium that groups fibers together in sheets an average of 4 ± 2 myocytes thick ($48 \pm 20\ \mu$m), separated by histologically distinct cleavage planes [17–19]. LeGrice and colleagues [19] investigated these structures in a detailed morphometric study of four dog hearts. They describe an ordered laminar arrangement of myocytes with extensive cleavage planes running approximately radially from endocardium toward epicardium in transmural section. Like the fibers, the sheets also have a branching pattern with the number of branches varying considerably through the wall thickness. Recent reports suggest that, in addition to fiber orientations, diffusion tensor MRI may be able to detect laminar sheet orientations [20]. The tensor of diffusion coefficients in the myocardium detected by MRI has shown to be

orthotropic, and the principal axis of slowest diffusion was seen to coincide with the direction normal to the sheet planes.

The fibrous architecture of the myocardium has motivated models of myocardial material symmetry as transversely isotropic. The transverse laminae are the first structural evidence for material orthotropy and have motivated the development of models describing the variation of fiber, sheet, and sheet-normal axes throughout the ventricular wall [21]. This has led to the idea that the laminar architecture of the ventricular myocardium affects the significant transverse shears [22] and myofiber rearrangement [18] described in the intact heart during systole. By measuring three-dimensional distributions of strain across the wall thickness using biplane radiography of radiopaque markers, LeGrice and colleagues [23] found that the cleavage planes coincide closely with the planes of maximum shearing during ejection, and that the consequent reorientation of the myocytes may contribute 50% or more of normal systolic wall thickening. Arts et al. [24] showed that the distributions of sheet orientations measured within the left ventricular wall of the dog heart coincided closely with those predicted from observed three-dimensional wall strains using the assumption that laminae are oriented in planes that contain the muscle fibers and maximize interlaminar shearing. This assumption also leads to the conclusion that two families of sheet orientations may be expected. Indeed, a retrospective analysis of the histology supported this prediction and more recent observations confirm the presence of two distinct populations of sheet plane in the inner half of the ventricular wall.

A detailed description of the morphogenesis of the muscle fiber system in the developing heart is not available but there is evidence of an organized myofiber pattern by day 12 in the fetal mouse heart that is similar to that seen at birth (day 20) [25]. Abnormalities of cardiac muscle fiber patterns have been described in some disease conditions. In hypertrophic cardiomyopathy, which is often familial, there is substantial myofiber disarray, typically in the interventricular septum [10,26].

54.2.3 Extracellular Matrix Organization

The cardiac extracellular matrix consists primarily of the fibrillar collagens, type I (85%) and III (11%), synthesized by the cardiac fibroblasts, the most abundant cell type in the heart. Collagen is the major structural protein in connective tissues, but only comprises 2 to 5% of the myocardium by weight, compared with the myocytes, which make up 90% [27]. The collagen matrix has a hierarchical organization (Figure 54.3), and has been classified according to conventions established for skeletal muscle into endomysium, perimysium, and epimysium [28,29]. The endomysium is associated with individual cells and includes a fine weave surrounding the cell and transverse structural connections 120 to 150 nm long connecting adjacent myocytes, with attachments localized near the z-line of the sarcomere. The primary purpose of the endomysium is probably to maintain registration between adjacent cells. The perimysium groups cells together and includes the collagen fibers that wrap bundles of cells into the laminar sheets described above as well as large coiled fibers typically 1 to 3μm in diameter composed of smaller collagen fibrils (40 to 50 nm) [30]. The helix period of the coiled perimysial fibers is about 20μm and the convolution index (ratio of fiber arclength to midline length) is approximately 1.3 in the unloaded state of the ventricle [31,32]. These perimysial fibers are most likely to be the major structural elements of the collagen extracellular matrix though they probably contribute to myocardial strain energy by uncoiling rather than stretching [31]. Finally, a thick epimysial collagen sheath surrounds the entire myocardium forming the protective epicardium (visceral pericardium) and endocardium.

Collagen content, organization, cross-linking and ratio of types I to III change with age and in various disease conditions including myocardial ischemia and infarction, hypertension and hypertrophy (Table 54.4). Changes in myocardial collagen content and organization coincide with alterations in diastolic myocardial stiffness [33]. Collagen intermolecular cross-linking is mediated by two separate mechanisms. The formation of enzymatic hydroxylysyl pyridinoline cross-links is catalyzed by lysyl oxidase, which requires copper as a cofactor. Nonenzymatic collagen cross-links known as advanced glycation endproducts can be formed in the presence of reducing sugars. This mechanism has been seen to significantly increase ventricular wall stiffness independent of changes in tissue collagen content, not only in

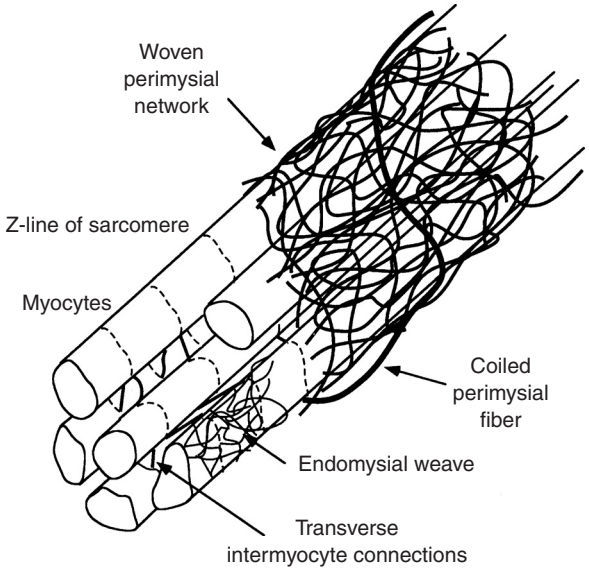

FIGURE 54.3 Schematic representation of cardiac tissue structure showing the association of endomysial and perimysial collagen fibers with cardiac myocytes. (Courtesy Dr. Deidre MacKenna.)

TABLE 54.4 Changes in Ventricular Collagen Structure and Mechanics with Age and Disease

Condition	Collagen morphology	Types and crosslinking	Passive stiffness	Other
Pressure overload hypertrophy	[Hydroxyproline]: ⇑-⇑⇑⇑ [132,133]	Type III: ⇑ [135]	Chamber: ⇑-⇑⇑ [133,134]	Perivascular fibrosis ⇑⇑ [133]
	Area fraction: ⇑⇑⇑ [133,134]	Cross-links: no change [136]	Tissue: ⇑⇑ [137]	Focal scarring: [138,139]
Volume overload hypertrophy	[Hydroxyproline]: no change-⇓: [140,141]	Cross-links: ⇑ [136,141]	Chamber: ⇓ [143]	Parallel changes
	Area Fraction: no change [132,142]	Type III/I: ⇑ [141]	Tissue: no change/⇑ [143]	
Acute ischemia/stunning	[Hydroxyproline]: ⇓ [Charney 1992 #1118]		⇓ early [146] ⇑ late [147]	Collagenase activity: ⇑ [148,149]
	Light microscopy: no change/⇓ [144] ⇓⇓ endomysial fibers [145]			
Chronic myocardial infarction	[Hydroxyproline]: ⇑⇑⇑ [150,151]	Type III: ⇑ [153]	Chamber: ⇑ early [154]	Organization: ⇑-⇑⇑⇑ [155,156]
	Loss of birefringence [152]		Chamber: ⇓ late [154]	
Age	[Hydroxyproline]: ⇑-⇑⇑⇑ [148,157]	Type III/I: ⇓ [158]	Chamber: ⇑ [159]	Light microscopy: fibril diameter ⇑ [157]
	Collagen fiber diameter ⇑ [157]	Cross-links: ⇑ [158]	Papillary muscle: ⇑ [160]	

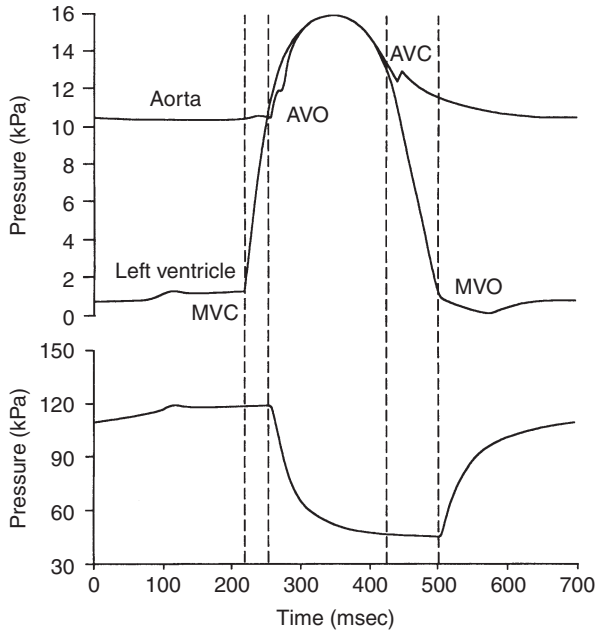

FIGURE 54.4 Left ventricular pressure, aortic pressure, and left ventricular volume during a single cardiac cycle showing the times of mitral valve closure (MVC), aortic valve opening (AVO), aortic valve closure (AVC) and mitral valve opening (MVO).

diabetics, but also in an animal model of volume overload hypertrophy [34]. Hence the collagen matrix plays an important role in determining the elastic material properties of the ventricular myocardium.

54.3 Cardiac Pump Function

54.3.1 Ventricular Hemodynamics

The most basic mechanical parameters of the cardiac pump are blood pressure and volume flowrate, especially in the major pumping chambers, the ventricles. From the point of view of wall mechanics, the ventricular pressure is the most important boundary condition. Schematic representations of the time-courses of pressure and volume in the left ventricle are shown in Figrue 54.4. Ventricular filling immediately following mitral valve opening (MVO) is initially rapid because the ventricle produces a diastolic suction as the relaxing myocardium recoils elastically from its compressed systolic configuration below the resting chamber volume. The later slow phase of ventricular filling (diastasis) is followed finally by atrial contraction. The deceleration of the inflowing blood reverses the pressure gradient across the valve leaflets and causes them to close mital valve closure (MVC). Valve closure may not, however, be completely passive, because the atrial side of the mitral valve leaflets, which unlike the pulmonic and aortic valves are cardiac in embryological origin, have muscle and nerve cells, and are electrically coupled to atrial conduction [35].

Ventricular contraction is initiated by excitation, which is almost synchronous (the duration of the QRS complex of the ECG is only about 60 msec in the normal adult) and begins about 0.1 to 0.2 sec after atrial depolarization. Pressure rises rapidly during the isovolumic contraction phase (about 50 msec in adult humans), and the aortic valve opens (AVO) when the developed pressure exceeds the aortic pressure (afterload). Most of the cardiac output is ejected within the first quarter of the ejection phase before the pressure has peaked. The aortic valve closes (AVC) 20 to 30 msec after AVO when the ventricular pressure falls below the aortic pressure owing to the deceleration of the ejecting blood. The dichrotic

notch, a characteristic feature of the aortic pressure waveform and a useful marker of aortic valve closure, is caused by pulse wave reflections in the aorta. Since the pulmonary artery pressure against which the right ventricle pumps is much lower than the aortic pressure, the pulmonic valve opens before and closes after the aortic valve. The ventricular pressure falls during isovolumic relaxation, and the cycle continues. The rate of pressure decay from the value P_0 at the time of the peak rate of pressure fall until MVO is commonly characterized by a single exponential time constant, that is,

$$P(t) = P_0 e^{-t/\tau} + P_\infty, \tag{54.7}$$

where P_∞ is the (negative) baseline pressure to which the ventricle would eventually relax if MVO were prevented [36]. In dogs and humans, τ is normally about 40 msec, but it is increased by various factors including elevated afterload, asynchronous contraction associated with abnormal activation sequence or regional dysfunction, and slowed cytosolic calcium reuptake to the sarcoplasmic reticulum associated with cardiac hypertrophy and failure. The pressure and volume curves for the right ventricle look essentially the same; however, the right ventricular and pulmonary artery pressures are only about a fifth of the corresponding pressures on the left side of the heart. The intraventricular septum separates the right and left ventricles and can transmit forces from one to the other. An increase in right ventricular volume may increase the left ventricular pressure by deformation of the septum. This direct interaction is most significant during filling [37].

The phases of the cardiac cycle are customarily divided into systole and diastole. The end of diastole — the start of systole — is generally defined as the time of MVC. Mechanical end-systole is usually defined as the end of ejection, but Brutsaert and colleagues proposed extending systole until the onset of diastasis (see the review by Brutsaert and Sys [38]), since there remains considerable myofilament interaction and active tension during relaxation. The distinction is important from the point of view of cardiac muscle mechanics: the myocardium is still active for much of diastole and may never be fully relaxed at sufficiently high heart rates (over 150 beats per minute). Here, we will retain the traditional definition of diastole, but consider the ventricular myocardium to be "passive" or "resting" only in the final slow-filling stage of diastole.

54.3.2 Ventricular Pressure–Volume Relations and Energetics

A useful alternative to Figure 54.4 for displaying ventricular pressure and volume changes is the pressure–volume loop shown in Figure 54.5(a). During the last 20 years, the ventricular pressure–volume relationship has been explored extensively, particularly by Sagawa, and colleagues [39], who wrote a comprehensive book on the approach. The isovolumic phases of the cardiac cycle can be recognized as the vertical segments of the loop, the lower limb represents ventricular filling, and the upper segment is the ejection phase. The difference on the horizontal axis between the vertical isovolumic segments is the stroke volume, which expressed as a fraction of the end-diastolic volume is the ejection fraction. The effects of altered loading on the ventricular pressure–volume relation have been studied in many preparations, but the best controlled experiments have used the isolated cross-circulated canine heart in which the ventricle fills and ejects against a computer-controlled volume servo-pump.

Changes in the filling pressure of the ventricle (preload) move the end-diastolic point along the unique end-diastolic pressure–volume relation (EDPVR), which represents the passive filling mechanics of the chamber that are determined primarily by the thick-walled geometry and nonlinear elasticity of the resting ventricular wall. Alternatively, if the afterload seen by the left ventricle is increased, stroke volume decreases in a predictable manner. The locus of end-ejection points (AVC) forms the end-systolic pressure–volume relation (ESPVR), which is approximately linear in a variety of conditions and also largely independent of the ventricular load history. Hence, the ESPVR is almost the same for isovolumic beats as for ejecting beats, although consistent effects of ejection history have been well characterized [40]. Connecting pressure–volume points at corresponding times in the cardiac cycle also results in a relatively linear relationship throughout systole with the intercept on the volume axis V_0 remaining nearly constant (Figure 54.5[b]).

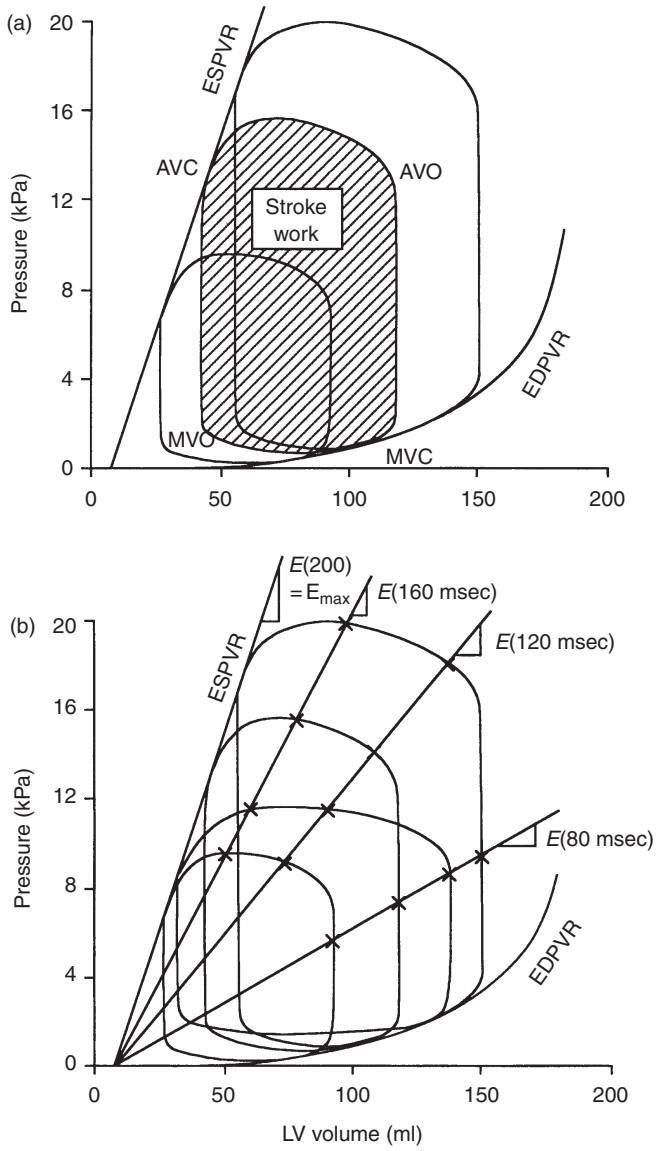

FIGURE 54.5 Schematic diagram of left ventricular pressure–volume loops: (a) End-systolic pressure–volume relation (ESPVR), end-diastolic pressure–volume relation (EDPVR) and stroke work. The three P–V loops show the effects of changes in preload and afterload. (b) Time-varying elastance approximation of ventricular pump function (see text).

This leads to the valuable approximation that the ventricular volume $V(t)$ at any instance during systole is simply proportional to the instantaneous pressure $P(t)$ through a time-varying elastance $E(t)$:

$$P(t) = E(t)\{V(t) - V_0\} \tag{54.8}$$

The maximum elastance $E_{\max}$, the slope of the ESPVR, has acquired considerable significance as an index of cardiac contractility that is independent of ventricular loading conditions. As the inotropic state of the myocardium increases, for example with catecholamine infusion, $E_{\max}$ increases, and with a negative inotropic effect such as a reduction in coronary artery pressure, it decreases.

The area of the ventricular pressure–volume loop is the external work (EW) performed by the myocardium on the ejecting blood:

$$\mathrm{EW} = \int_{\mathrm{EDV}}^{\mathrm{ESV}} P(t)\mathrm{d}V \tag{54.9}$$

Plotting this stroke work against a suitable measure of preload gives a ventricular function curve, which illustrates the single most important intrinsic mechanical property of the heart pump. In 1914, Patterson and Starling [41] performed detailed experiments on the canine heart–lung preparation, and Starling summarized their results with his famous "Law of the Heart", which states that the work output of the heart increases with ventricular filling. The so-called Frank–Starling mechanism is now well recognized to be an intrinsic mechanical property of cardiac muscle (see Section 54.4).

External stroke work is closely related to cardiac energy utilization. Since myocardial contraction is fueled by ATP, 90 to 95% of which is normally produced by oxidative phosphorylation, cardiac energy consumption is often studied in terms of myocardial oxygen consumption, VO_2 (ml $O_2.g^{-1}.beat^{-1}$). Since energy is also expended during nonworking contractions, Suga and colleagues [42] defined the pressure–volume area (PVA) ($J.g^{-1}.beat^{-1}$) as the loop area (external stroke work) plus the end-systolic potential energy (internal work), which is the area under the ESPVR left of the isovolumic relaxation line (Figure 54.5[a]),

$$\mathrm{PVA} = \mathrm{EW} + \mathrm{PE} \tag{54.10}$$

The PVA has strong linear correlation with VO_2 independent of ejection history. Equation (54.11) has typical values for the dog heart:

$$VO_2 = 0.12(\mathrm{PVA}) + 2.0 \times 10^{-4} \tag{54.11}$$

The intercept represents the sum of the oxygen consumption for basal metabolism and the energy associated with activation of the contractile apparatus, which is primarily used to cycle intracellular Ca^{2+} for excitation–contraction coupling [42]. The reciprocal of the slope is the contractile efficiency [43,44]. The VO_2–PVA relation shifts its elevation but not its slope with increments in E_{max} with most positive and negative inotropic interventions [43,45–48]. However, ischemic-reperfused viable but "stunned" myocardium has a smaller O_2 cost of PVA [49].

Although the PVA approach has also been useful in many settings, it is fundamentally phenomenological. Because the time-varying elastance assumptions ignores the well-documented load-history dependence of cardiac muscle tension, [50–52] theoretical analyses that attempt to reconcile PVA with crossbridge mechanoenergetics [53] are usually based on isometric or isotonic contractions. So that regional oxygen consumption in the intact heart can be related to myofiber biophysics, regional variations on the pressure–volume area have been proposed, such as the tension-area area [54], normalization of E_{max} [55], and the fiber stress-strain area [56].

In mammals, there are characteristic variations in cardiac function with heart size. In the power law relation for heart rate as a function of body mass (analogous to Equation [54.3]), the coefficient k is 241 $beats.min^{-1}$ and the power α is -0.25 [5]. In the smallest mammals, like soricine shrews that weigh only a few grams, maximum heart rates exceeding 1000 $beats.min^{-1}$ have been measured [57]. Ventricular cavity volume scales linearly with heart weight, and ejection fraction and blood pressure are reasonably invariant from rats to horses. Hence, stroke work also scales directly with heart size [58], and thus work rate and energy consumption would be expected to increase with decreased body size in the same manner as heart rate. However, careful studies have demonstrated only a twofold increase in myocardial heat production as body mass decreases in mammals ranging from humans to rats, despite a 4.6-fold increase in heart rate [59]. This suggests that cardiac energy expenditure does not scale in proportion to heart rate and that cardiac metabolism is a lower proportion of total body metabolism in the smaller species.

The primary determinants of the EDPVR are the material properties of resting myocardium, the chamber dimensions and wall thickness, and the boundary conditions at the epicardium, endocardium, and valve annulus [60]. The EDPVR has been approximated by an exponential function of volume (see e.g.,

chapter 9 in Gaasch and Lewinter [61]), though a cubic polynomial also works well. Therefore, the passive chamber stiffness dP/dV is approximately proportional to the filling pressure. Important influences on the EDPVR include the extent of relaxation, ventricular interaction and pericardial constraints, and coronary vascular engorgement. The material properties and boundary conditions in the septum are important since they determine how the septum deforms [62,63]. Through septal interaction, the EDPVR of the left ventricle may be directly affected by changes in the hemodynamic loading conditions of the right ventricle. The ventricles also interact indirectly since the output of the right ventricle is returned as the input to the left ventricle via the pulmonary circulation. Slinker and Glantz [64], using pulmonary artery and venae caval occlusions to produce direct (immediate) and indirect (delayed) interaction transients, concluded that the direct interaction is about half as significant as the indirect coupling. The pericardium provides a low friction mechanical enclosure for the beating heart that constrains ventricular overextension [65] Since the pericardium has stiffer elastic properties than the ventricles [66], it contributes to direct ventricular interactions. The pericardium also augments the mechanical coupling between the atria and ventricles [67]. Increasing coronary perfusion pressure has been seen to increase the slope of the diastolic pressure–volume relation (an "erectile" effect) [68,69].

54.4 Myocardial Material Properties

54.4.1 Muscle Contractile Properties

Cardiac muscle mechanics testing is far more difficult than skeletal muscle testing mainly owing to the lack of ideal test specimens like the long single fiber preparations that have been so valuable for studying the mechanisms of skeletal muscle mechanics. Moreover, under physiological conditions, cardiac muscle cannot be stimulated to produce sustained tetanic contractions due to the absolute refractory period of the myocyte cell membrane. Cardiac muscle also exhibits a mechanical property analogous to the relative refractory period of excitation. After a single isometric contraction, some recovery time is required before another contraction of equal amplitude can be activated. The time constant for this mechanical restitution property of cardiac muscle is about 1 sec [70].

Unlike skeletal muscle, in which maximal active force generation occurs at a sarcomere length that optimizes myofilament overlap ($\sim$2.1 μm), the isometric twitch tension developed by isolated cardiac muscle continues to rise with increased sarcomere length in the physiological range (1.6 to 2.4 μm) (Figure 54.6[a]). Early evidence for a descending limb of the cardiac muscle isometric length–tension

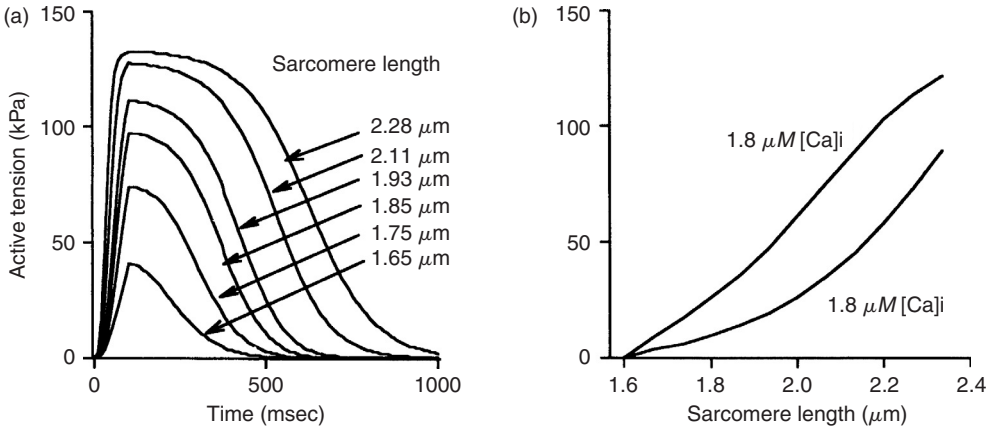

FIGURE 54.6 Cardiac muscle isometric twitch tension generated by a model of rat cardiac contraction (courtesy Dr. Julius Guccione): (a) Developed twitch tension as a function of time and sarcomere length; (b) Peak isometric twitch tension vs. sarcomere length for low and high calcium concentration.

curve was found to be caused by shortening in the central region of the isolated muscle at the expense of stretching at the damaged ends where specimen was tethered to the test apparatus. If muscle length is controlled so that sarcomere length in the undamaged part of the muscle is indeed constant, or if the developed tension is plotted against the instantaneous sarcomere length rather than the muscle length, the descending limb is eliminated [71]. Thus, the increase with chamber volume of end-systolic pressure and stroke work is reflected in isolated muscle as a monotonic increase in peak isometric tension with sarcomere length (Figure 54.6[b]). Note that the active tension shown in Figure 54.6 is the total tension minus the resting tension, which, unlike in skeletal muscle, becomes very significant at sarcomere lengths over 2.3 μm. The increase in slope of the ESPVR associated with increased contractility is mirrored by the effects of increased calcium concentration in the length–tension relation. The duration as well as the tension developed in the active cardiac twitch also increases substantially with sarcomere length (Figure 54.6[a]).

The relationship between cytosolic calcium concentration and isometric muscle tension has mostly been investigated in muscle preparations in which the sarcolemma has been chemically permeabilized. Because there is evidence that this chemical "skinning" alters the calcium sensitivity of myofilament interaction, recent studies have also investigated myofilament calcium sensitivity in intact muscles tetanized by high-frequency stimulation in the presence of a compound such as ryanodine that open calcium release sites in the sarcoplasmic reticulum. Intracellular calcium concentration was estimated using calcium-sensitive optical indicators such as Fura. The myofilaments are activated in a graded manner by micromolar concentrations of calcium, which binds to troponin-C according to a sigmoidal relation [72]. Half-maximal tension in cardiac muscle is developed at intracellular calcium concentrations of 10^{-6} to 10^{-5} M (the C_{50}) depending on factors such as species and temperature [70]. Hence, relative isometric tension $T_0/T_{\max}$ may be modeled using [73,74].

$$\frac{T_0}{T_{\max}} = \frac{[\mathrm{Ca}]^n}{[\mathrm{Ca}]^n + C_{50}^n} \tag{54.12}$$

The Hill coefficient (n) governs the steepness of the sigmoidal curve. A wide variety of values have been reported but most have been in the range 3 to 6 [75–78]. The steepness of the isometric length–tension relation (Figure 54.6[b]), compared with that of skeletal muscle is due to length-dependent calcium sensitivity. That is, the C_{50} (M) and n both change with sarcomere length, L (μm). Hunter et al. [74] used the following approximations to fit the data of Kentish et al. [76] from rat right ventricular trabeculae:

$$n = 4.25\{1 + 1.95(L/L_{\mathrm{ref}} - 1)\}, \quad \mathrm{pC}_{50} = -\log_{10}\mathrm{C}_{50} = 5.33\{1 + 0.31(L/L_{\mathrm{ref}} - 1)\} \tag{54.13}$$

where the reference sarcomere length L_{ref} was taken to be 2.0 μm.

The isotonic force–velocity relation of cardiac muscle is similar to that of skeletal muscle, and A.V. Hill's well-known hyperbolic relation is a good approximation except at larger forces greater than about 85% of the isometric value. The maximal (unloaded) velocity of shortening is essentially independent of preload, but does change with time during the cardiac twitch and is affected by factors that affect contractile ATPase activity and hence crossbridge cycling rates. de-Tombe and ter Keurs [79] using sarcomere length-controlled isovelocity release experiments found that viscous forces imposes a significant internal load-opposing sarcomere shortening. If the isotonic shortening response is adjusted for the confounding effects of passive viscoelasticity, the underlying crossbridge force–velocity relation is found to be linear.

AQ: Please check the change of 'De Tombe and colleagues' to 'de Tombe and ter Keurs'.

Cardiac muscle contraction also exhibits other significant length-history-dependent properties. An important example is "deactivation" associated with length transients. The isometric twitch tension redeveloped following a brief length transient that dissociates crossbridges, reaches the original isometric value when the transient is imposed early in the twitch before the peak tension is reached. But following transients applied at times after the peak twitch tension has occurred, the fraction of tension redeveloped declines progressively since the activator calcium has fallen to levels below that necessary for all crossbridges to reattach [80].

There have been many model formulations of cardiac muscle contractile mechanics, too numerous to summarize here. In essence they may be grouped into three categories. Time-varying elastance models include the essential dependence of cardiac active force development on muscle length and time. These models would seem to be well suited to the continuum analysis of whole heart mechanics [1,81,82] by virtue of the success of the time-varying elastance concept of ventricular function (see Section 54.3.2). In "Hill" models the active fiber stress development is modified by shortening or lengthening according to the force–velocity relation, so that fiber tension is reduced by increased shortening velocity [83,84]. Fully history-dependent models are more complex and are generally based on A.F. Huxley's crossbridge theory [52,85–87]. A statistical approach known as the distribution moment model has also been shown to provide an excellent approximation to crossbridge theory [88]. An alternative more phenomenological approach is Hunter's fading memory theory, which captures the complete length-history dependence of cardiac muscle contraction without requiring all the biophysical complexity of crossbridge models [74]. The appropriate choice of model will depend on the purpose of the analysis. For many models of global ventricular function, a time-varying elastance model will suffice, but for an analysis of sarcomere dynamics in isolated muscle or the ejecting heart, a history-dependent analysis is more appropriate.

Although Hill's basic assumption that resting and active muscle fiber tension are additive is axiomatic in one-dimensional tests of isolated cardiac mechanics, there remains little experimental information on how the passive and active material properties of myocardium superpose in two or three dimensions. The simplest and commonest assumption is that active stress is strictly one-dimensional and adds to the fiber component of the three-dimensional passive stress. However, even this addition will indirectly affect all the other components of the stress response, since myocardial elastic deformations are finite, nonlinear and approximately isochoric (volume conserving). In an interesting and important new development, biaxial testing of tetanized and barium-contracted ventricular myocardium has shown that developed systolic stress also has a large component in directions transverse to the mean myofiber axis that can exceed 50% of the axial fiber component [89]. The magnitude of this transverse active stress depended significantly on the biaxial loading conditions. Moreover, evidence from osmotic swelling and other studies suggests that transverse strain can affect contractile tension development along the fiber axis by altering myofibril lattice spacing [90,91]. The mechanisms of transverse active stress development remain unclear but two possible contributors are the geometry of the crossbridge head itself, which is oriented oblique to the myofilament axis [92], and the dispersion of myofiber orientation [10].

54.4.2 Resting Myocardial Properties

Since, by the Frank–Starling mechanism, end-diastolic volume directly affects systolic ventricular work, the mechanics of resting myocardium also have fundamental physiological significance. Most biomechanics studies of passive myocardial properties have been conducted in isolated, arrested whole heart or tissue preparations. Passive cardiac muscle exhibits most of the mechanical properties characteristic of soft tissues in general [93]. In cyclic uniaxial loading and unloading, the stress–strain relationship is nonlinear with small but significant hysteresis. Depending on the preparation used, resting cardiac muscle typically requires from 2 to 10 repeated loading cycles to achieve a reproducible (preconditioned) response. Intact cardiac muscle experiences finite deformations during the normal cardiac cycle, with maximum Lagrangian strains (which are generally radial and endocardial) that may easily exceed 0.5 in magnitude. Hence, the classical linear theory of elasticity is quite inappropriate for resting myocardial mechanics. The hysteresis of the tissue is consistent with a viscoelastic response, which is undoubtedly related to the substantial water content of the myocardium (about 80% by mass). Changes in water content, such as edema, can cause substantial alterations in the passive stiffness and viscoelastic properties of myocardium. The viscoelasticity of passive cardiac muscle has been characterized in creep and relaxation studies of papillary muscle from cat and rabbit. In both species, the tensile stress in response to a step in strain relaxes 30 to 40% in the first 10 seconds [94,95]. The relaxation curves exhibit a short exponential time constant ($<$0.02 sec) and a long one (about 1000 sec), and are largely independent of the strain magnitude, which supports the approximation that myocardial viscoelasticity is quasilinear. Myocardial

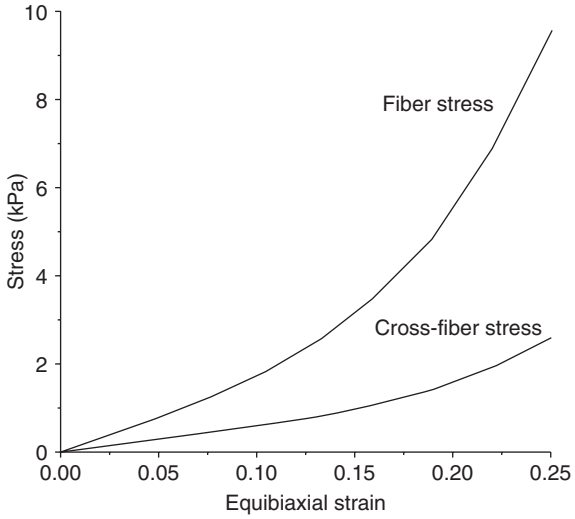

FIGURE 54.7 Representative stress–strain curves for passive rat myocardium computed using Equations (17) and (19). Fiber and crossfiber stress are shown for equibiaxial strain. (Courtesy Dr. Jeffrey Omens.)

creep under isotonic loading is 2 to 3% of the original length after 100 sec of isotonic loading and is also quasilinear with an exponential timecourse. There is also evidence that passive ventricular muscle exhibits other anelastic properties such as maximum-strain-dependent "strain softening" [96,97], a well-known property in elastomers first described by Mullins [98].

Since the hysteresis of passive cardiac muscle is small and only weakly affected by changes in strain rate, the assumption of pseudoelasticity [93] is often appropriate. That is, the resting myocardium is considered to be a finite elastic material with different elastic properties in loading vs. unloading. Although various preparations have been used to study resting myocardial elasticity, the most detailed and complete information has come from biaxial and multiaxial tests of isolated sheets of cardiac tissue, mainly from the dog [99–101]. These experiments have shown that the arrested myocardium exhibits significant anisotropy with substantially greater stiffness in the muscle fiber direction than transversely. In equibiaxial tests of muscle sheets cut from planes parallel to the ventricular wall, fiber stress was greater than the transverse stress (Figure 54.7) by an average factor of close to 2.0 [102]. Moreover, as suggested by the structural organization of the myocardium described in Section 54.2, there may also be significant anisotropy in the plane of the tissue transverse to the fiber axis.

The biaxial stress–strain properties of passive myocardium display some heterogeneity. Recently, Novak et al. [103] measured regional variations of biaxial mechanics in the canine left ventricle. Specimens from the inner and outer thirds of the left ventricular free wall were stiffer than those from the midwall and interventricular septum, but the degree of anisotropy was similar in each region. Significant species variations in myocardial stiffness have also been described. Using measurements of two-dimensional regional strain during left ventricular inflation in the isolated whole heart, a parameter optimization approach showed that canine cardiac tissue was several times stiffer than that of the rat, though the nonlinearity and anisotropy were similar [104]. Biaxial testing of the collagenous parietal pericardium and epicardium have shown that these tissues have distinctly different properties than the myocardium being very compliant and isotropic at low-biaxial strains ($<$0.1 to 0.15) but rapidly becoming very stiff and anisotropic as the strain is increased [66,100].

Various constitutive models have been proposed for the elasticity of passive cardiac tissues. Because of the large deformations and nonlinearity of these materials, the most useful framework has been provided by the pseudostrain-energy formulation for hyperelasticity. For a detailed review of the material properties of passive myocardium and approaches to constitutive modeling, the reader is referred to chapters 1 to 6

of Glass et al [105]. In hyperelasticity, the components of the stress* are obtained from the strain energy W as a function of the Lagrangian (Green's) strain E_{RS}.

The myocardium is generally assumed to be an incompressible material, which is a good approximation in the isolated tissue, although in the intact heart there can be a significant redistribution of tissue volume associated with phasic changes in regional coronary blood volume. Incompressibility is included as a kinematic constraint in the finite elasticity analysis, which introduces a new pressure variable that is added as a Lagrange multiplier in the strain energy. The examples that follow are various strain–energy functions, with representative parameter values (for W in kPa, i.e., mJ.ml^{-1}) that have been suggested for cardiac tissues. For the two-dimensional properties of canine myocardium, Yin and colleagues [102] obtained reasonable fits to experimental data with an exponential function,

$$W = 0.47\mathrm{e}^{(35E_{11}^{1,2}+20E_{22}^{1,2})} \tag{54.14}$$

where E_{11} is the fiber strain and E_{22} is the crossfiber in-plane strain. Humphrey and Yin [106] proposed a three-dimensional form for W as the sum of an isotropic exponential function of the first principal invariant I_1 of the right Cauchy–Green deformation tensor and another exponential function of the fiber stretch ratio λ_F:

$$W = 0.21\left(\mathrm{e}^{9.4(I_1-3)} - 1\right) + 0.35\left(\mathrm{e}^{66(\lambda_F-1)^2} - 1\right), \tag{54.15}$$

The isotropic part of this expression has also been used to model the myocardium of the embryonic chick heart during the ventricular looping stages, with coefficients of 0.02 kPa during diastole and 0.78 kPa at end-systole, and exponent parameters of 1.1 and 0.85, respectively [107]. Another related transversely isotropic strain-energy function was used by Guccione et al. [108] and Omens et al. [109] to model material properties in the isolated mature rat and dog hearts:

$$W = 0.6(\mathrm{e}Q - 1), \tag{54.16}$$

where, in the dog

$$Q = 26.7E_{11}^2 + 2.0(E_{22}^2 + E_{33}^2 + E_{23}^2 + E_{32}^2) + 14.7(E_{12}^2 + E_{21}^2 + E_{13}^2 + E_{31}^2), \tag{54.17}$$

and, in the rat

$$Q = 9.2E_{11}^2 + 2.0(E_{22}^2 + E_{33}^2 + E_{23}^2 + E_{32}^2) + 3.7(E_{12}^2 + E_{21}^2 + E_{13}^2 + E_{31}^2). \tag{54.18}$$

In Equations (54.17) and (54.18), normal and shear strain components involving the radial (x_3) axis are included. Humphrey and colleagues [110] determined a new polynomial form directly from biaxial tests. Novak et al. [103] gave representative coefficients for canine myocardium from three layers of the left ventricular free wall. For the outer third, they obtained

$$W = 4.8(\lambda_F - 1)^2 + 3.4(\lambda_F - 1)^3 + 0.77(I_1 - 3) - 6.1(I_1 - 3)(\lambda_F - 1) + 6.2(I_1 - 3)^2, \tag{54.19}$$

for the midwall region

$$W = 5.3(\lambda_F - 1)^2 + 7.5(\lambda_F - 1)^3 + 0.43(I_1 - 3) - 7.7(I_1 - 3)(\lambda_F - 1) + 5.6(I_1 - 3)^2, \tag{54.20}$$

and for the inner layer of the wall

$$W = 0.51(\lambda_F - 1)^2 + 27.6(\lambda_F - 1)^3 + 0.74(I_1 - 3) - 7.3(I_1 - 3)(\lambda_F - 1) + 7.0(I_1 - 3)^2. \tag{54.21}$$

* In a hyperelastic material, the *second Piola Kirchhoff* stress tensor is given by, $P_{RS}1/2((\partial W/\partial E_{RS}) + (\partial W/\partial E_{SR}))$.

A power law strain–energy function expressed in terms of circumferential, longitudinal and transmural extension ratios (λ_1, λ_2, and λ_3) was used [111] to describe the biaxial properties of sheep myocardium 2 weeks after experimental myocardial infarction, in the scarred infarct region:

$$W = 0.36\left(\frac{\lambda_1^{32}}{32} + \frac{\lambda_2^{30}}{30} + \frac{\lambda_3^{31}}{31} - 3\right) \tag{54.22}$$

and in the remote, noninfarcted tissue:

$$W = 0.11\left(\frac{\lambda_1^{22}}{22} + \frac{\lambda_2^{26}}{26} + \frac{\lambda_3^{24}}{24} - 3\right) \tag{54.23}$$

Finally, based on the observation that resting stiffness rises steeply at strains that extend coiled collagen fibers to the limit of uncoiling, Hunter and colleagues have proposed a pole-zero constitutive relation in which the stresses rise asymptotically as the strain approaches a limiting elastic strain [74].

The strain in the constitutive equation must generally be referred to the stress-free state of the tissue. However, the unloaded state of the passive left ventricle is not stress-free; residual stress exists in the intact, unloaded myocardium, as shown by Omens and Fung [112]. Cross-sectional equatorial rings from potassium-arrested rat hearts spring open elastically when the left ventricular wall is resected radially. The average opening angle of the resulting curved arc is $45 \pm 10°$ in the rat. Subsequent radial cuts produce no further change. Hence, a slice with one radial cut is considered to be stress-free, and there is a nonuniform distribution of residual strain across the intact wall, being compressive at the endocardium and tensile at the epicardium, with some regional differences. Stress analyses of the diastolic left ventricle have shown that residual stress acts to minimize the endocardial stress concentrations that would otherwise be associated with diastolic loading [108]. An important physiological consequence of residual stress is that sarcomere length is nonuniform in the unloaded resting heart. Rodriguez et al. [113] showed that sarcomere length is about 0.13 μm greater at epicardium than endocardium in the unloaded rat heart, and this gradient vanishes when residual stress is relieved. Three-dimensional studies have also revealed the presence of substantial transverse residual shear strains [114]. Residual stress and strain may have an important relationship to cardiac growth and remodeling. Theoretical studies have shown that residual stress in tissues can arise from growth fields that are kinematically incompatible [115,116].

54.5 Regional Ventricular Mechanics: Stress and Strain

Although ventricular pressures and volumes are valuable for assessing the global pumping performance of the heart, myocardial stress and strain distributions are needed to characterize regional ventricular function, especially in pathological conditions, such as myocardial ischemia and infarction, where profound localized changes may occur. The measurement of stress in the intact myocardium involves resolving the local forces acting on defined planes in the heart wall. Attempts to measure local forces [117,118] have had limited success because of the large deformations of the myocardium and the uncertain nature of the mechanical coupling between the transducer elements and the tissue. Efforts to measure intramyocardial pressures using miniature implanted transducers have been more successful but have also raised controversy over the extent to which they accurately represent changes in interstitial fluid pressure. In all cases, these methods provide an incomplete description of three-dimensional wall stress distributions. Therefore, the most common approach for estimating myocardial stress distributions is the use of mathematical models based on the laws of continuum mechanics. Although there is no room to review these analyses here, the important elements of such models are the geometry and structure, boundary conditions, and material properties, described in the foregoing sections. An excellent review of ventricular wall stress analysis is given by Yin [119]. The most versatile and powerful method for ventricular stress analysis is

the finite element method, which has been used in cardiac mechanics for over 20 years [120]. However, models must also be validated with experimental measurements. Since the measurement of myocardial stresses is not yet reliable, the best experimental data for model validation are measurements of strains in the ventricular wall.

The earliest myocardial strain gauges were mercury-in-rubber transducers sutured to the epicardium. These days, local segment length changes are routinely measured with various forms of the piezoelectric crystal sonomicrometer. However, since the ventricular myocardium is a three-dimensional continuum, the local strain is only fully defined by all the normal and shear components of the myocardial strain tensor. Villarreal et al. [121] measured two-dimensional midwall strain components by arranging three piezoelectric crystals in a small triangle so that three segment lengths could be measured simultaneously. They showed that the principal axis of greatest shortening is not aligned with circumferential midwall fibers, and that this axis changes with altered ventricular loading and contractility. Therefore, uniaxial segment measurements do not reveal the full extent of alterations in regional function caused by an experimental intervention. Another approach to measuring regional myocardial strains is the use of clinical imaging techniques, such as contrast ventriculography, high-speed x-ray tomography, MRI or two-dimensional echocardiography. But the conventional application of these techniques is not suitable for measuring regional strains because they cannot be used to identify the motion of distinct myocardial points. They only produce a profile or silhouette of a surface, except in the unusual circumstance when radiopaque markers are implanted in the myocardium during cardiac surgery or transplantation [122]. Hunter and Zerhouni [123] describe the prospects for noninvasive imaging of discrete points in the ventricular wall. The most promising method is the use of MRI tagging methods, which are now being used to map three-dimensional ventricular strain fields in conscious subjects [4].

In experimental research, implantable radiopaque markers are used for tracking myocardial motions with high spatial and temporal resolution. Meier et al. [124,125] placed triplets of metal markers 10 to 15 mm apart near the epicardium of the canine right ventricle and reconstructed their positions from biplane cinéradiographic recordings. By polar decomposition, they obtained the two principal epicardial strains, the principal angle, and the local rotation in the region. The use of radiopaque markers was extended to three dimensions by Waldman and colleagues [22], who implanted three closely separated columns of 5 to 6 metal beads in the ventricular wall. With this technique, it is possible to find all six components of strain and all three rigid-body rotation angles at sites through the wall. For details of this method, see the review by Waldman in chapter 7 of Glass et al [105]. An enhancement to this method uses high-order finite element interpolation of the marker positions to compute continuous transmural distributions of myocardial deformation [126].

Studies and models such as these are producing an increasingly detailed picture of regional myocardial stress and strain distributions. Of the many interesting observations, there are some useful generalizations, particularly regarding the strain. Myocardial deformations are large and three dimensional, and hence the nonlinear finite strain tensors are more appropriate measures than the linear infinitesimal Cauchy strain. During filling in the normal heart, the wall stretches biaxially but nonuniformly in the plane of the wall, and thins in the transmural direction. During systole, shortening is also two dimensional and the wall thickens. There are substantial regional differences in the timecourse, magnitude, and pattern of myocardial deformations. In humans and dogs, in-plane systolic myocardial shortening and diastolic lengthening vary with longitudinal position on the left and right ventricular free walls generally increasing in magnitude from base to apex.

Both during systole and diastole, there are significant shear strains in the wall. In-plane (torsional) shears are negative during diastole, consistent with a small left-handed torsion of the left ventricle during filling, and positive as the ventricular twist reverses during ejection. Consequently, the principal axes of greatest diastolic segment lengthening and systolic shortening are not circumferential or longitudinal but at oblique axes, which are typically rotated 10 to 60° clockwise from circumferential. There are circumferential variations in regional left ventricular strain. The principal axes of greatest diastolic lengthening and systolic shortening tend to be more longitudinal on the posterior wall and more circumferentially oriented on the anterior wall. Perhaps the most significant regional variations are transmural. In-plane

and transmural, normal or principal strains, are usually significantly greater in magnitude at the endocardium than the epicardium both in filling and ejection. However, when the strain is resolved in the local muscle fiber direction, the transmural variation of fiber strain becomes insignificant. The combination of torsional deformation and the transmural variation in fiber direction means that systolic shortening and diastolic lengthening tend to be maximized in the fiber direction at the epicardium and minimized at the endocardium. Hence, whereas maximum shortening and lengthening are closely aligned with muscle fibers at the subepicardium, they are almost perpendicular to the fibers at the subendocardium. In the left ventricular wall there are also substantial transverse shear strains (i.e., in the circumferential-radial and longitudinal-radial planes) during systole, though during filling they are smaller. Their functional significance remains unclear, though they change substantially during acute myocardial ischemia or ventricular pacing and are apparently associated with the transverse laminae described earlier [23].

Sophisticated continuum mechanics models are needed to determine the stress distributions associated with these complex myocardial deformations. With modern finite element methods it is now possible to include in the analysis the three-dimensional geometry and fiber architecture, finite deformations, nonlinear material properties, and muscle contraction of the ventricular myocardium. Some models have included other factors such as viscoelasticity, poroelasticity, coronary perfusion, growth and remodeling, regional ischemia, residual stress and electrical activation. To date, continuum models have provided some valuable insight into regional cardiac mechanics. These include the importance of muscle fiber orientation, torsional deformations and residual stress, and the substantial inhomogeneities associated with regional variations in geometry and fiber angle or myocardial ischemia and infarction. A new arena in which models promise to make important contributions is the rapidly growing field of cardiac resynchronization therapy [127]. The use of biventricular pacing in cases of congestive heart failure that are accompanied by electrical conduction asynchrony has been seen to significantly improve ventricular pump function. However the improvement in mechanical function is not well predicted by the improvement in electrical synchrony. New electromechanical models promise to provide insights into the mechanisms of cardiac resynchronization therapy and potentially to optimize the pacing protocols used [128].

Acknowledgments

I am indebted to many colleagues and students, past and present, for their input and perspective of cardiac biomechanics. Owing to space constraints, I have relied on much of their work without adequate citation, especially in the final section. Special thanks to Drs. Jeffrey Omens, Deidre MacKenna, Julius Guccione, and Jyoti Rao.

References

[1] Taber, L.A., On a nonlinear theory for muscle shells. Part II — application to the beating left ventricle, *ASME J. Biomech. Eng.*, 113, 63–71, 1991.

[2] Streeter, D.D., Jr. and Hanna, W.T., Engineering mechanics for successive states in canine left ventricular myocardium: I. Cavity and wall geometry, *Circ. Res.*, 33, 639–655, 1973.

[3] Nielsen, P.M.F., Le Grice, I.J., Smaill, B.H., et al., Mathematical model of geometry and fibrous structure of the heart, *Am. J. Physiol.*, 260, H1365–H1378, 1991.

[4] Young, A.A. and Axel, L., Three-dimensional motion and deformation in the heart wall: estimation from spatial modulation of magnetization — a model-based approach, *Radiology*, 185, 241–247, 1992.

[5] Stahl, W.R., Scaling of respiratory variable in mammals, *J. Appl. Physiol.*, 22, 453–460, 1967.

[6] Rakusan, K., Cardiac growth, maturation and aging, in *Growth of the Heart in Health and Disease*, R. Zak, Ed. Raven Press, New York: 1984, pp. 131–164.

[7] Streeter, D.D., Jr., Gross morphology and fiber geometry of the heart, in *Handbook of Physiology, Section 2: The Cardiovascular System, Chapter 4*, I, B. R. M, Ed. American Physiological Society, Bethesda, MD: 1979, pp. 61–112.

[8] Saffitz, J.E., Kanter, H.L., Green, K.G., et al., Tissue-specific determinants of anisotropic conduction velocity in canine atrial and ventricular myocardium, *Circ. Res.*, 74, 1065–1070, 1994.
[9] Torrent-Guasp, F., *The Cardiac Muscle* Juan March Foundation, 1973.
[10] Karlon, W.J., Covell, J.W., McCulloch, A.D., et al., Automated measurement of myofiber disarray in transgenic mice with ventricular expression of ras, *Anat. Rec.*, 252, 612–625, 1998.
[11] Streeter, D.D., Jr., Spotnitz, H.M., Patel, D.P., et al., Fiber orientation in the canine left ventricle during diastole and systole, *Circ. Res.*, 24, 339–347, 1969.
[12] Vetter, F.J. and McCulloch, A.D., Three-dimensional analysis of regional cardiac function: a model of rabbit ventricular anatomy, *Prog. in Biophys. Mol. Biol.*, 69, 157–183, 1998.
[13] Hsu, E.W., Muzikant, A.L., Matulevicius, S.A., et al., Magnetic resonance myocardial fiber-orientation mapping with direct histological correlation, *Am. J. Physiol.*, 274, H1627–H1634, 1998.
[14] Scollan, D.F., Holmes, A., Winslow, R., et al., Histological validation of myocardial microstructure obtained from diffusion tensor magnetic resonance imaging, *Am. J. Physiol.*, 275, H2308–H2318, 1998.
[15] Dou, J., Tseng, W.Y., Reese, T.G., et al., Combined diffusion and strain MRI reveals structure and function of human myocardial laminar sheets in vivo, *Magn. Reson. Med.*, 50, 107–113, 2003.
[16] McCulloch, A.D., Smaill, B.H., and Hunter, P.J., Regional left ventricular epicardial deformation in the passive dog heart, *Circ. Res.*, 64, 721–733, 1989.
[17] Smaill, B.H. and Hunter, P.J., Structure and function of the diastolic heart, in *Theory of Heart*, L. Glass, P. J. Hunter, and A. D. McCulloch, Eds. Springer-Verlag, New York: 1991, pp. 1–29.
[18] Spotnitz, H.M., Spotnitz, W.D., Cottrell, T.S., et al., Cellular basis for volume related wall thickness changes in the rat left ventricle, *J. Mol. Cell Cardiol.*, 6, 317–331, 1974.
[19] LeGrice, I.J., Smaill, B.H., Chai, L.Z., et al., Laminar structure of the heart: ventricular myocyte arrangement and connective tissue architecture in the dog, *Am. J. Physiol.*, 269, H571–H582, 1995.
[20] Tseng, W.Y., Wedeen, V.J., Reese, T.G., et al., Diffusion tensor MRI of myocardial fibers and sheets: correspondence with visible cut-face texture, *J. Magn. Reson. Imaging*, 17, 31–42, 2003.
[21] Legrice, I.J., Hunter, P.J., and Smaill, B.H., Laminar structure of the heart: a mathematical model, *Am. J. Physiol.*, 272, H2466–H2476, 1997.
[22] Waldman, L.K., Fung, Y.C., and Covell, J.W., Transmural myocardial deformation in the canine left ventricle: normal in vivo three-dimensional finite strains, *Circ. Res.*, 57, 152–163, 1985.
[23] LeGrice, I.J., Takayama, Y., and Covell, J.W., Transverse shear along myocardial cleavage planes provides a mechanism for normal systolic wall thickening, *Circ. Res.*, 77, 182–193, 1995.
[24] Arts, T., Costa, K.D., Covell, J.W., et al., Relating myocardial laminar architecture to shear strain and muscle fiber orientation, *Am. J. Physiol. Heart Circ. Physiol.*, 280, H2222–H2229, 2001.
[25] McLean, M., Ross, M.A., and Prothero, J., Three-dimensional reconstruction of the myofiber pattern in the fetal and neonatal mouse heart, *Anat. Rec.*, 224, 392–406, 1989.
[26] Maron, B.J., Bonow, R.O., Cannon, R.O.D., et al., Hypertrophic cardiomyopathy. Interrelations of clinical manifestations, pathophysiology, and therapy (1), *N. Engl. J. Med.*, 316, 780–789, 1987.
[27] Weber, K.T., Cardiac interstituim in health and disease: the fibrillar collagen network, *J. Am. Coll. Cardiol.*, 13, 1637–165, 1989.
[28] Robinson, T.F., Cohen-Gould, L., and Factor, S.M., Skeletal framework of mammalian heart muscle: arrangement of inter- and pericellular connective tissue structures, *Lab. Invest.*, 49, 482–498, 1983.
[29] Caulfield, J.B. and Borg, T.K., The collagen network of the heart, *Lab. Invest.*, 40, 364–371, 1979.
[30] Robinson, T.F., Geraci, M.A., Sonnenblick, E.H., et al., Coiled perimysial fibers of papillary muscle in rat heart: morphology, distribution, and changes in configuration, *Circ. Res.*, 63, 577–592, 1988.
[31] MacKenna, D.A., Omens, J.H., and Covell, J.W., Left ventricular perimysial collagen fibers uncoil rather than stretch during diastolic filling, *Basic Res. Cardiol.*, 91, 111–22, 1996.
[32] MacKenna, D.A., Vaplon, S.M., and McCulloch, A.D., Microstructural model of perimysial collagen fibers for resting myocardial mechanics during ventricular filling, *Am. J. Physiol.*, 273, H1576–H1586, 1997.

[33] MacKenna, D.A. and McCulloch, A.D., Contribution of the collagen extracellular matrix to ventricular mechanics, in *Systolic and Diastolic Function of the Heart*, N.B. Ingels, G.T. Daughters, J. Baan, J.W. Covell, R.S. Reneman, and F.C.-P. Yin, Eds. IOS Press, Amsterdam: 1996, pp. 35–46.

[34] Herrmann, K.L., McCulloch, A.D., and Omens, J.H., Glycated collagen cross-linking alters cardiac mechanics in volume-overload hypertrophy, *Am. J. Physiol. Heart Circ. Physiol.*, 284, H1277–H1284, 2003.

[35] Sonnenblick, E.H., Napolitano, L.M., Daggett, W.M., et al., An intrinsic neuromuscular basis for mitral valve motion in the dog, *Circ. Res.*, 21, 9–15, 1967.

[36] Yellin, E.L., Hori, M., Yoran, C., et al., Left ventricular relaxation in the filling and nonfilling intact canine heart, *Am. J. Physiol.*, 250, H620–H629, 1986.

[37] Janicki, J.S. and Weber, K.T., The pericardium and ventricular interaction, distensibility and function, *Am. J. Physiol.*, 238, H494–H503, 1980.

[38] Brutsaert, D.L. and Sys, S.U., Relaxation and diastole of the heart, *Physiol. Rev.*, 69, 1228, 1989.

[39] Sagawa, K., Maughan, L., Suga, H., et al., *Cardiac Contraction and the Pressure–Volume Relationship*. Oxford University Press, 1988.

[40] Hunter, W.C., End-systolic pressure as a balance between opposing effects of ejection, *Circ. Res.*, 64, 265–275, 1989.

[41] Patterson, S.W. and Starling, E.H., On the mechanical factors which determine the output of the ventricles, *J. Physiol.*, 48, 357–379, 1914.

[42] Suga, H., Hayashi, T., and Shirahata, M., Ventricular systolic pressure–volume area as predictor of cardiac oxygen consumption, *Am. J. Physiol.*, 240, H39–H44, 1981.

[43] Suga, H. and Goto, Y., Cardiac oxygen costs of contractility (Emax) and mechanical energy (PVA): new key concepts in cardiac energetics, in *Recent Progress in Failing Heart Syndrome*, S. Sasayama and H. Suga, Eds. Springer-Verlag, Tokyo: 1991, pp. 61–115.

[44] Suga, H., Goto, Y., Kawaguchi, O., et al., Ventricular perspective on efficiency, *Basic Research in Cardiology*, 88 (Suppl 2), 43–65, 1993.

[45] Suga, H., Ventricular energetics, *Physiol. Rev.*, 70, 247–277, 1990.

[46] Suga, H., Goto, Y., Yasumura, Y., et al., O2 consumption of dog heart under decreased coronary perfusion and propranolol, *Am. J. Physiol.*, 254, H292–H303, 1988.

[47] Zhao, D.D., Namba, T., Araki, J., et al., Nipradilol depresses cardiac contractility and O2 consumption without decreasing coronary resistance in dogs, *Acta. Med. Okayama.*, 47, 29–33, 1993.

[48] Namba, T., Takaki, M., Araki, J., et al., Energetics of the negative and positive inotropism of pentobarbitone sodium in the canine left ventricle, *Cardiovascular. Res.*, 28, 557–564, 1994.

[49] Ohgoshi, Y., Goto, Y., Futaki, S., et al., Increased oxygen cost of contractility in stunned myocardium of dog, *Circulat. Res.*, 69, 975–988, 1991.

[50] Burkhoff, D., Schnellbacher, M., Stennett, R.A., et al., Explaining load-dependent ventricular performance and energetics based on a model of E-C coupling, in *Cardiac Energetics: from Emax to Pressure–Volume Area*, M.M. LeWinter, H. Suga, and M.W. Watkins, Eds. Kluwer Academic Publishers, Boston: 1995.

[51] ter Keurs, H.E. and de Tombe, P.P., Determinants of velocity of sarcomere shortening in mammalian myocardium, *Adv. Exp. Med. Biol.*, 332, 649–664; discussion 664–665, 1993.

[52] Guccione, J.M. and McCulloch, A.D., Mechanics of active contraction in cardiac muscle: Part I — Constitutive relations for fiber stress that describe deactivation, *J. Biomech. Eng.*, 115, 72–81, 1993.

[53] Taylor, T.W., Goto, Y., and Suga, H., Variable cross-bridge cycling-ATP coupling accounts for cardiac mechanoenergetics, *Am. J. Physiol.*, 264, H994–H1004, 1993.

[54] Goto, Y., Futaki, S., Kawaguchi, O., et al., Coupling between regional myocardial oxygen consumption and contraction under altered preload and afterload, *J. Am. Coll. Cardiol.*, 21, 1522–1531, 1993.

[55] Sugawara, M., Kondoh, Y., and Nakano, K., Normalization of Emax and PVA, in *Cardiac Energetics: From Emax to Pressure–Volume Area*, M.M. LeWinter, H. Suga, and M.W. Watkins, Eds. Kluwer Academic Publishers, Boston: 1995, pp. 65–78.
[56] Delhaas, T., Arts, T., Prinzen, F.W., et al., Regional fibre stress-fibre strain area as an estimate of regional blood flow and oxygen demand in the canine heart, *J. Physiol. (Lond.)*, 477, 481–496, 1994.
[57] Vornanen, M., Maximum heart rate of sorcine shrews: correlation with contractile properties and myosin composition, *Am. J. Physiol.*, 31, R842–R851, 1992.
[58] Holt, J.P., Rhode, E.A., Peoples, S.A., et al., Left ventricular function in mammals of greatly different size, *Circ. Res.*, 10, 798–806, 1962.
[59] Loiselle, D.S. and Gibbs, C.L., Species differences in cardiac energetics, *Am. J. Physiol.*, 237, 1979.
[60] Gilbert, J.C. and Glantz, S.A., Determinants of left ventricular filling and of the diastolic pressure–volume relation, *Circ. Res.*, 64, 827–852, 1989.
[61] Gaasch, W.H. and LeWinter, M.M., *Left Ventricular Diastolic Dysfunction and Heart Failure*. Lea & Febiger, Philadelphia, PA: 1994.
[62] Glantz, S.A., Misbach, G.A., Moores, W.Y., et al., The pericardium substantially affects the left ventricular diastolic pressure–volume relationship in the dog, *Circ. Res.*, 42, 433–441, 1978.
[63] Glantz, S.A. and Parmley, W.W., Factors which affect the diastolic pressure–volume curve, *Circ. Res.*, 42, 171–180, 1978.
[64] Slinker, B.K. and Glantz, S.A., End-systolic and end-diastolic ventricular interaction, *Am. J. Physiol.*, 251, H1062–H1075, 1986.
[65] Mirsky, I. and Rankin, J.S., The effects of geometry, elasticity, and external pressures on the diastolic pressure–volume and stiffness-stress relations: How important is the pericardium? *Circ. Res.*, 44, 601–611, 1979.
[66] Lee, M.C., Fung, Y.C., Shabetai, R., et al., Biaxial mechanical properties of human pericardium and canine comparisons, *Am. J. Physiol.*, 253, H75–H82, 1987.
[67] Maruyama, Y., Ashikawa, K., Isoyama, S., et al., Mechanical interactions between the four heart chambers with and without the pericardium in canine hearts, *Circ. Res.*, 50, 86–100, 1982.
[68] May-Newman, K., Omens, J.H., Pavelec, R.S., et al., Three-dimensional transmural mechanical interaction between the coronary vasculature and passive myocardium in the dog, *Circ. Res.*, 74, 1166–1178, 1994.
[69] Salisbury, P.F., Cross, C.E., and Rieben, P.A., Influence of coronary artery pressure upon myocardial elasticity, *Circ. Res.*, 8, 794–800, 1960.
[70] Bers, D.M., *Excitation-Contraction Coupling and Cardiac Contractile Force*. Kluwer, 1991.
[71] ter Keurs, H.E.D.J., Rijnsburger, W.H., van Heuningen, R., et al., Tension development and sarcomere length in rat cardiac trabeculae: evidence of length-dependent activation, *Circ. Res.*, 46, 703–713, 1980.
[72] Rüegg, J.C., *Calcium in Muscle Activation: A Comparative Approach*, 2nd ed. Springer-Verlag, 1988.
[73] Tözeren, A., Continuum rheology of muscle contraction and its application to cardiac contractility, *Biophys. J.*, 47, 303–309, 1985.
[74] Hunter, P.J., McCulloch, A.D., and ter Keurs, H.E., Modelling the mechanical properties of cardiac muscle, *Prog. Biophys. Mol. Biol.*, 69, 289–331, 1998.
[75] Backx, P.H., Gao, W.D., Azan-Backx, M.D., et al., The relationship between contractile force and intracellular [Ca2+] in intact rat cardiac trabeculae, *J. Gen. Physiol.*, 105, 1–19, 1995.
[76] Kentish, J.C., Ter Keurs, H.E.D.J., Ricciari, L., et al., Comparisons between the sarcomere length–force relations of intact and skinned trabeculae from rat right ventricle, *Circ. Res.*, 58, 755–768, 1986.
[77] Yue, D.T., Marban, E., and Wier, W.G., Relationship between force and intracellular [Ca2+] in tetanized mammalian heart muscle, *J. Gen. Physiol.*, 87, 223–242, 1986.
[78] Gao, W.D., Backx, P.H., Azan-Backx, M., et al., Myofilament Ca2+ sensitivity in intact versus skinned rat ventricular muscle, *Circ. Res.*, 74, 408–415, 1994.

AQ: Please provide publisher location for reference [70].

[79] de Tombe, P.P. and ter Keurs, H.E., An internal viscous element limits unloaded velocity of sarcomere shortening in rat myocardium, *J. Physiol. (Lond.)*, 454, 619–642, 1992.
[80] ter Keurs, H.E.D.J., Rijnsburger, W.H., and van Heuningen, R., Restoring forces and relaxation of rat cardiac muscle, *Eur. Heart. J.*, 1, 67–80, 1980.
[81] Arts, T., Reneman, R.S., and Veenstra, P.C., A model of the mechanics of the left ventricle, *Ann. Biomed. Eng.*, 7, 299–318, 1979.
[82] Chadwick, R.S., Mechanics of the left ventricle, *Biophys. J.*, 39, 279–288, 1982.
[83] Nevo, E. and Lanir, Y., Structural finite deformation model of the left ventricle during diastole and systole, *J. Biomech. Eng.*, 111, 342–349, 1989.
[84] Arts, T., Veenstra, P.C., and Reneman, R.S., Epicardial deformation and left ventricular wall mechanics during ejection in the dog, *Am. J. Physiol.*, 243, H379–H390, 1982.
[85] Panerai, R.B., A model of cardiac muscle mechanics and energetics, *J. Biomech.*, 13, 929–940, 1980.
[86] Landesberg, A., Markhasin, V.S., Beyar, R., et al., Effect of cellular inhomogeneity on cardiac tissue mechanics based on intracellular control mechanisms, *Am. J. Physiol.*, 270, H1101–H1114, 1996.
[87] Landesberg, A. and Sideman, S., Coupling calcium binding to troponin C and cross-bridge cycling in skinned cardiac cells, *Am. J. Physiol.*, 266, H1260–H1271, 1994.
[88] Ma, S.P. and Zahalak, G.I., A distribution-moment model of energetics in skeletal muscle [see comments], *J. Biomech.*, 24, 21–35, 1991.
[89] Lin, D.H.S. and Yin, F.C.P., A multiaxial constitutive law for mammalian left ventricular myocardium in steady-state barium contracture or tetanus, *J. Biomech. Eng.*, 120, 504–517, 1998.
[90] Schoenberg, M., Geometrical factors influencing muscle force development. I. The effect of filament spacing upon axial forces, *Biophys. J.*, 30, 51–67, 1980.
[91] Zahalak, G.I., Non-axial muscle stress and stiffness, *J. Theor. Biol.*, 182, 59–84, 1996.
[92] Schoenberg, M., Geometrical factors influencing muscle force development. II. Radial forces, *Biophys. J.*, 30, 69–77, 1980.
[93] Fung, Y.C., *Biomechanics: Mechanical Properties of Living Tissues*, 2nd ed. Springer-Verlag, Inc., 1993.
[94] Pinto, J.G. and Patitucci, P.J., Creep in cardiac muscle, *Am. J. Physiol.*, 232, H553–H563, 1977.
[95] Pinto, J.G. and Patitucci, P.J., Visco-elasticity of passive cardiac muscle, *J. Biomech. Eng.*, 102, 57–61, 1980.
[96] Emery, J.L., Omens, J.H., and McCulloch, A.D., Strain softening in rat left ventricular myocardium, *J. Biomech. Eng.*, 119, 6–12, 1997.
[97] Emery, J.L., Omens, J.H., and McCulloch, A.D., Biaxial mechanics of the passively overstretched left ventricle, *Am. J. Physiol.*, 272, H2299–H2305, 1997.
[98] Mullins, L., Effect of stretching on the properties of rubber, *J. Rubber Res.*, 16, 275–289, 1947.
[99] Halperin, H.R., Chew, P.H., Weisfeldt, M.L., et al., Transverse stiffness: a method for estimation of myocardial wall stress, *Circ. Res.*, 61, 695–703, 1987.
[100] Humphrey, J.D., Strumpf, R.K., and Yin, F.C.P., Biaxial mechanical behavior of excised ventricular epicardium, *Am. J. Physiol.*, 259, H101–H108, 1990.
[101] Demer, L.L. and Yin, F.C.P., Passive biaxial mechanical properties of isolated canine myocardium, *J. Physiol.*, 339, 615–630, 1983.
[102] Yin, F.C.P., Strumpf, R.K., Chew, P.H., et al., Quantification of the mechanical properties of noncontracting canine myocardium under simultaneous biaxial loading, *J. Biomech.*, 20, 577–589, 1987.
[103] Novak, V.P., Yin, F.C.P., and Humphrey, J.D., Regional mechanical properties of passive myocardium, *J. Biomech.*, 27, 403–412, 1994.
[104] Omens, J.H., MacKenna, D.A., and McCulloch, A.D., Measurement of strain and analysis of stress in resting rat left ventricular myocardium, *J. Biomech.*, 26, 665–676, 1993.
[105] Glass, L., Hunter, P., and McCulloch, A.D., Theory of Heart: Biomechanics, Biophysics and Nonlinear Dynamics of Cardiac Function, in *Institute for Nonlinear Science*, H. Abarbanel, Ed. Springer-Verlag, New York, 1991.

AQ: Please provide publisher location for reference [93].

[106] Humphrey, J.D. and Yin, F.C.P., A new constitutive formulation for characterizing the mechanical behavior of soft tissues, *Biophys. J.*, 52, 563–570, 1987.
[107] Lin, I.-E. and Taber, L.A., Mechanical effects of looping in the embryonic chick heart, *J. Biomech.*, 27, 311–321, 1994.
[108] Guccione, J.M., McCulloch, A.D., and Waldman, L.K., Passive material properties of intact ventricular myocardium determined from a cylindrical model, *J. Biomech. Eng.*, 113, 42–55, 1991.
[109] Omens, J.H., MacKenna, D.A., and McCulloch, A.D., Measurement of two-dimensional strain and analysis of stress in the arrested rat left ventricle, *Adv. Bioeng.*, BED-20, 635–638, 1991.
[110] Humphrey, J.D., Strumpf, R.K., and Yin, F.C.P., Determination of a constitutive relation for passive myocardium: I. A New functional form, *J. Biomech. Eng.*, 112, 333–339, 1990.
[111] Gupta, K.B., Ratcliff, M.B., Fallert, M.A., et al., Changes in passive mechanical stiffness of myocardial tissue with aneurysm formation, *Circulation*, 89, 2315–2326, 1994.
[112] Omens, J.H. and Fung, Y.C., Residual strain in rat left ventricle, *Circ. Res.*, 66, 37–45, 1990.
[113] Rodriguez, E.K., Omens, J.H., Waldman, L.K., et al., Effect of residual stress on transmural sarcomere length distribution in rat left ventricle, *Am. J. Physiol.*, 264, H1048–H1056, 1993.
[114] Costa, K., May-Newman, K., Farr, D., et al., Three-dimensional residual strain in canine mid-anterior left ventricle, *Am. J. Physiol.*, 273, H1968–H1976, 1997.
[115] Skalak, R., Dasgupta, G., Moss, M., et al., Analytical description of growth, *J. Theor. Biol.*, 94, 555–577, 1982.
[116] Rodriguez, E.K., Hoger, A., and McCulloch, A.D., Stress-dependent finite growth in soft elastic tissues, *J. Biomech.*, 27, 455–467, 1994.
[117] Feigl, E.O., Simon, G.A., and Fry, D.L., Auxotonic and isometric cardiac force transducers, *J. Appl. Physiol.*, 23, 597–600, 1967.
[118] Huisman, R.M., Elzinga, G., Westerhof, N., et al., Measurement of left ventricular wall stress, *Cardiovasc. Res.*, 14, 142–153, 1980.
[119] Yin, F.C.P., Ventricular wall stress, *Circ. Res.*, 49, 829–842, 1981.
[120] Yin, F.C.P., Applications of the finite-element method to ventricular mechanics, *CRC Crit. Rev. Biomed. Eng.*, 12, 311–342, 1985.
[121] Villarreal, F.J., Waldman, L.K., and Lew, W.Y.W., Technique for measuring regional two-dimensional finite strains in canine left ventricle, *Circ. Res.*, 62, 711–721, 1988.
[122] Ingels, N.B., Jr., Daughters, G.T., II, Stinson, E.B., et al., Measurement of midwall myocardial dynamics in intact man by radiography of surgically implanted markers, *Circulation*, 52, 859–867, 1975.
[123] Hunter, W.C. and Zerhouni, E.A., Imaging distinct points in left ventricular myocardium to study regional wall deformation, in *Innovations in Diagnostic Radiology*, J.H. Anderson, Ed. Springer-Verlag, New York: 1989, 169–190.
[124] Meier, G.D., Bove, A.A., Santamore, W.P., et al., Contractile function in canine right ventricle, *Am. J. Physiol.*, 239, H794–H804, 1980.
[125] Meier, G.D., Ziskin, M.C., Santamore, W.P., et al., Kinematics of the beating heart, *IEEE Trans. Biomed. Eng.*, 27, 319–329, 1980.
[126] McCulloch, A.D. and Omens, J.H., Non-homogeneous analysis of three-dimensional transmural finite deformations in canine ventricular myocardium, *J. Biomech.*, 24, 539–548, 1991.
[127] Leclercq, C., Faris, O., Tunin, R., et al., Systolic improvement and mechanical resynchronization does not require electrical synchrony in the dilated failing heart with left bundle-branch block, *Circulation*, 106, 1760–1763, 2002.
[128] Usyk, T.P. and McCulloch, A.D., Electromechanical model of cardiac resynchronization in the dilated failing heart with left bundle branch block, *J. Electrocardiol.*, 36, 57–61, 2003.
[129] Ross, J., Jr., Sonnenblick, E.H., Covell, J.W., et al., The architecture of the heart in systole and diastole: technique of rapid fixation and analysis of left ventricular geometry, *Circ. Res.*, 21, 409–421, 1967.

[130] Grossman, W., Cardiac hypertrophy: useful adaptation or pathologic process? *Am. J. Med.*, 69, 576–583, 1980.
[131] Grossman, W., Jones, D., and McLaurin, L.P., Wall stress and patterns of hypertrophy in the human left ventricle, *J. Clin. Invest.*, 56, 56–64, 1975.
[132] Medugorac, I., Myocardial collagen in different forms of hypertrophy in the rat, *Res. Exp. Med. (Berl.)*, 177, 201–211, 1980.
[133] Weber, K.T., Janicki, J.S., Shroff, S.G., et al., Collagen remodeling of the pressure-overloaded, hypertrophied nonhuman primate myocardium, *Circ. Res.*, 62, 757–65, 1988.
[134] Jalil, J.E., Doering, C.W., Janicki, J.S., et al., Structural vs. contractile protein remodeling and myocardial stiffness in hypertrophied rat left ventricle, *J. Mol. Cell. Cardiol.*, 20, 1179–87, 1988.
[135] Mukherjee, D. and Sen, S., Collagen phenotypes during development and regression of myocardial hypertrophy in spontaneously hypertensive rats, *Circ. Res.*, 67, 1474–1480, 1990.
[136] Harper, J., Harper, E., and Covell, J.W., Collagen characterization in volume-overload- and pressure-overload-induced cardiac hypertrophy in minipigs, *Am. J. Physiol.*, 265, H434–H438, 1993.
[137] Omens, J.H., Milkes, D.E., and Covell, J.W., Effects of pressure overload on the passive mechanics of the rat left ventricle, *Ann. Biomed. Eng.*, 23, 152–163, 1995.
[138] Contard, F., Koteliansky, V., Marotte, F., et al., Specific alterations in the distribution of extracellular matrix components within rat myocardium during the development of pressure overload, *Lab. Invest.*, 64, 65–75, 1991.
[139] Silver, M.A., Pick, R., Brilla, C.G., et al., Reactive and reparative fibrillar collagen remodelling in the hypertrophied rat left ventricle: two experimental models of myocardial fibrosis, *Cardiovasc. Res.*, 24, 741–747, 1990.
[140] Michel, J.B., Salzmann, J.L., Ossondo Nlom, M., et al., Morphometric analysis of collagen network and plasma perfused capillary bed in the myocardium of rats during evolution of cardiac hypertrophy, *Basic Res. Cardiol.*, 81, 142–154, 1986.
[141] Iimoto, D.S., Covell, J.W., and Harper, E., Increase in crosslinking of type I and type III collagens associated with volume overload hypertropy, *Circ. Res.*, 63, 399–408, 1988.
[142] Weber, K.T., Pick, R., Silver, M.A., et al., Fibrillar collagen and remodeling of dilated canine left ventricle, *Circulation*, 82, 1387–1401, 1990.
[143] Corin, W.J., Murakami, T., Monrad, E.S., et al., Left ventricular passive diastolic properties in chronic mitral regurgitation, *Circulation*, 83, 797–807, 1991.
[144] Whittaker, P., Boughner, D.R., Kloner, R.A., et al., Stunned myocardium and myocardial collagen damage: differential effects of single and repeated occlusions, *Am. Heart J.*, 121, 434–441, 1991.
[145] Zhao, M., Zhang, H., Robinson, T.F., et al., Profound structural alterations of the extracellular collagen matrix in postischemic dysfunctional ("stunned") but viable myocardium, *J. Am. Coll. Cardiol.*, 10, 1322–1334, 1987.
[146] Forrester, J.S., Diamond, G., Parmley, W.W., et al., Early increase in left ventricular compliance after myocardial infarction, *J. Clin. Invest.*, 51, 598–603, 1972.
[147] Pirzada, F.A., Ekong, E.A., Vokonas, P.S., et al., Experimental myocardial infarction XIII. Sequential changes in left ventricular pressure–length relationships in the acute phase, *Circulation*, 53, 970–975, 1976.
[148] Takahashi, S., Barry, A.C., and Factor, S.M., Collagen degradation in ischaemic rat hearts, *Biochem. J.*, 265, 233–241, 1990.
[149] Charney, R.H., Takahashi, S., Zhao, M., et al., Collagen loss in the stunned myocardium, *Circulation*, 85, 1483–1490, 1992.
[150] Connelly, C.M., Vogel, W.M., Wiegner, A.W., et al., Effects of reperfusion after coronary artery occlusion on post-infarction scar tissue, *Circ. Res.*, 57, 562–577, 1985.
[151] Jugdutt, B.I. and Amy, R.W., Healing after myocardial infarction in the dog: changes in infarct hydroxyproline and topography, *J. Am. Coll. Cardiol.*, 7, 91–102, 1986.

[152] Whittaker, P., Boughner, D.R., and Kloner, R.A., Analysis of healing after myocardial infarction using polarized light microscopy, *Am. J. Pathol.*, 134, 879–893, 1989.
[153] Jensen, L.T., Hørslev-Petersen, K., Toft, P., et al., Serum aminoterminal type III procollagen peptide reflects repair after acute myocardial infarction, *Circulation*, 81, 52–57, 1990.
[154] Pfeffer, J.M., Pfeffer, M.A., Fletcher, P.J., et al., Progressive ventricular remodeling in rat with myocardial infarction, *Am. J. Physiol.*, 260, H1406–H1414, 1991.
[155] Whittaker, P., Boughner, D.R., and Kloner, R.A., Role of collagen in acute myocardial infarct expansion, *Circulation*, 84, 2123–2134, 1991.
[156] Holmes, J.W., Yamashita, H., Waldman, L.K., et al., Scar remodeling and transmural deformation after infarction in the pig, *Circulation*, 90, 411–420, 1994.
[157] Eghbali, M., Robinson, T.F., Seifter, S., et al., Collagen accumulation in heart ventricles as a function of growth and aging, *Cardiovasc. Res.*, 23, 723–729, 1989.
[158] Medugorac, I. and Jacob, R., Characterisation of left ventricular collagen in the rat, *Cardiovasc. Res.*, 17, 15–21, 1983.
[159] Borg, T.K., Ranson, W.F., Moslehy, F.A., et al., Structural basis of ventricular stiffness, *Lab. Invest.*, 44, 49–54, 1981.
[160] Anversa, P., Puntillo, E., Nikitin, P., et al., Effects of age on mechanical and structural properties of myocardium of Fischer 344 rats, *Am. J. Physiol.*, 256, H1440–H1449, 1989.